CHEMISTRY OF MATERIALS
Article

Chem. Mater. **2010,** *22,* 3165–3173 3165
DOI:10.1021/cm100213a

$Li_3V(MoO_4)_3$: A New Material for Both Li Extraction and Insertion

D. Mikhailova,*[,†,‡] A. Sarapulova,[†] A. Voss,[†] A. Thomas,[†] S. Oswald,[†] W. Gruner,[†] D. M. Trots,[§] N. N. Bramnik,[‡] and H. Ehrenberg[†]

[†]*Institute for Complex Materials, IFW Dresden, Helmholtzstr. 20, D-01069 Dresden, Germany,* [‡]*Institute for Materials Science, Technische Universität Darmstadt, Petersenstr. 23, D-64287 Darmstadt, Germany, and* [§]*Bavarian Research Institute of Experimental Geochemistry and Geophysics, University of Bayreuth, Universitätsstr. 30, D-95440 Bayreuth, Germany*

Received January 22, 2010. Revised Manuscript Received March 28, 2010

Besides topotactical Li insertion, Li deinsertion also is possible for the new potential electrode material $Li_3V(MoO_4)_3$, in contrast to isostructural $Li_3Fe(MoO_4)_3$. This new phase crystallizes in an orthorhombic NASICON-type structure with large channels along the crystallographic *a*-axis, which are half-filled by Li atoms. A reversible reduction of $Li_3V(MoO_4)_3$ occurs at 2.1 V, with the formation of isostructural $Li_4V(MoO_4)_3$, whereas an oxidation to $Li_2V(MoO_4)_3$ is found at 3.7 V, preserving the space-group symmetry. The first charge/discharge cycle differs significantly from the following ones. According to X-ray photoelectron spectroscopy (XPS) measurements, Li extraction is associated with vanadium oxidation ($V^{3+} \rightleftharpoons V^{4+}$) and Li intercalation is accompanied mainly by molybdenum reduction ($Mo^{6+} \rightleftharpoons Mo^{5+}$), but also is partially associated with vanadium reduction ($V^{3+} \rightleftharpoons V^{2+}$). In situ synchrotron diffraction on a $Li_xV(MoO_4)_3$ cathode with $x \approx 3$ during the first discharge/charge cycle revealed a monotonous increase of the lattice volume and of the lattice parameter *a* during Li insertion from $x = 3$ to $x = 3.5$, but a multiphase mechanism for $3.5 \leq x \leq 4$. At $x \leq 2.95$, a monotonous decrease of the lattice volume was observed. The paramagnetic moments of $Li_xV(MoO_4)_3$ ($x = 2, 3, 4$) are smaller than the theoretical values, calculated for spin-only contributions from V^{4+}, V^{3+}, and V^{2+}, respectively, which might indicate the partially delocalized character of the V valence electrons.

Introduction

Complex Li,V-containing phosphates with NASICON structure have been intensively studied for a long time as lithium storage materials, because of the presence of large channels in the structure, which are sufficient for good Li-ion mobility, and the ability of V ions to adopt different oxidation states from +2 to +5.[1] The insertion/extraction of Li in such compounds is often topochemically between isostructural end-members. For example, lithium extraction from $Li_3V_2(PO_4)_3$ with $LiV_2(PO_4)_3$ formation occurs at a potential of ~3.8 V vs Li^+/Li and corresponds to the highest value for polyanionic frameworks with theoretical discharge capacity of ~130 mA h/g.[1] The complex molybdenum oxides $Li_2M_2(MoO_4)_3$ and $Li_3M(MoO_4)_3$ (M = Fe, Co, Ni) are isostructural and attracted recently attention, because of their ability for reversible Li insertion.[2−6] They crystallize also in a NASICON-type structure, which was first described for the Na,Co-containing molybdate with $NaCo_{2.31}(MoO_4)_3$ stoichiometry.[7] There are large channels along one crystallographic axis in the structure, which are occupied by either only Li atoms as in the case of $Li_3M(MoO_4)_3$ or by Li and M atoms as for $Li_2M_2(MoO_4)_3$. The structural similarity of $Li_2M_2(MoO_4)_3$ and $Li_3M(MoO_4)_3$ can be described as a heterovalent replacement $Li_2M_2(MoO_4)_3 \rightarrow Li_2(Li,M)(MoO_4)_3 \rightarrow Li_3M(MoO_4)_3$. The room-temperature ionic conductivity of $Li_3Cr(MoO_4)_3$, with only Li ions in the channels, is higher than for the isostructural compound $Li_2Mg_2(MoO_4)_3$, despite the same ionic conductivities of both compounds at elevated temperatures.[8]

For M, a 3d-transition-metal Li deinsertion and Li insertion is accompanied by a $M^{2+} \leftrightarrow M^{3+}$ oxidation−reduction reaction. A detailed electrochemical investigation of Li intercalation into $Li_3Fe(MoO_4)_3$ demonstrated a reversible process at 2.4 V with $Li_4Fe(MoO_4)_3$ formation and the existence of Fe^{2+}.[2] In situ synchrotron diffraction showed a complex Li intercalation mechanism with the formation of an intermediate phase.[3] At lower voltages, an irreversible process with a reduction of Mo ions was observed. $Li_2Co_2(MoO_4)_3$ and $Li_2Ni_2(MoO_4)_3$ are promising candidates for high-voltage cathodes with an open-cell voltage of ca. 4.9 V

*Author to whom correspondence should be addressed. Tel.: +49 351 4659846. Fax: +49 351 4659452. E-mail: d.mikhailova@ifw-dresden.de.

(1) *Lithium Batteries: Science and Technology*; Nazri, G.-A., Pistoia, G., Eds.; Springer Science + Business Media: Berlin, 2009; 708 pp.
(2) Alvarez-Vega, M.; Amador, U.; Arroyo de Dompablo, M. E. *J. Electrochem. Soc.* **2005**, *152*, A1306–A1311.
(3) Arroyo de Dompablo, M. E.; Alvarez-Vega, M.; Baehtz, C.; Amador, U. *J. Electrochem. Soc.* **2006**, *153*, A275–A281.
(4) Prabaharan, S. R. S.; Ramesh, S.; Michael, M. S.; Begam, K. M. *Mater. Chem. Phys.* **2004**, *87*, 318–326.
(5) Prabaharan, S. R. S.; Michael, M. S.; Begam, K. M. *Electrochem. Solid-State Lett.* **2004**, *7*, A416–A420.
(6) Begam, K. M.; Prabaharan, S. R. S. *J. Power Sources* **2006**, *159*, 319–322.
(7) Ibers, J. A.; Smith, G. W. *Acta Crystallogr.* **1964**, *17*, 190–197.
(8) Sebastian, L.; Piffard, Y.; Shukla, A. K.; Taulelle, F.; Gopalakrishnan, J. *J. Mater. Chem.* **2003**, *13*, 1797–1802.

Published on Web 04/21/2010

vs Li^+/Li for Co[5] and for Ni.[6] $Li_2M_2(MoO_4)_3$ can also be obtained by Li intercalation into the ternary lithium-free molybdates $M_2(MoO_4)_3$ with sufficient space in the structure.[9,10]

Reversible electrochemical intercalation/extraction was observed for $Li_xFe_2(MoO_4)_3$ for $0 \leq x \leq 1.7$. This range corresponds to changes of the Fe oxidation state from +3 to +2.15. The accompanied phase transition leads to a metastable $Li_2Fe_2(MoO_4)_3$ phase isostructural to the high-temperature modification of $Fe_2(MoO_4)_3$, which transforms into the NASICON-type structure at elevated temperature.[9]

Li insertion was also performed into $Co_2(MoO_4)_3$: more than 2 Li atoms per formula unit can be intercalated at 2.6 V, corresponding to a reduction from Co^{3+} to Co^{2+}, and at 2.2 V, assigned to a reduction of Mo^{6+}. A detailed investigation of the crystal structures of the involved phases during insertion is still lacking.[10] The reduction of Mo^{6+} in a NASICON-type structure seems to be irreversible in the most cases, perhaps caused by an instability of Mo^{5+} or Mo^{4+} in tetrahedral oxygen coordination.[9,10] In contrast, the recently investigated $Li_4Mo_5O_{17}$ phase[11] with MoO_6 octahedra only can insert eight Li ions reversibly and topotactically.

In the Li−Ti−Mo-O system, a new compound with Ti^{4+}, $Li_3Ti_{0.75}(MoO_4)_3$ with the same NASICON-type structure and vacancies in (□,Li,Ti)O_6-octahedra (4*c* site for Li and Ti), was recently prepared.[12] The mixed occupation of oxygen octahedra by Li^+ and Ti^{4+} is rather surprising, considering the very different charges of both cations, and indicates a pronounced stability of this structure type against Li extraction/insertion and accompanied valence changes.

The $Li_xV_y(MoO_4)_3$ system represents an interesting potential material for Li intercalation, because of the possibility for changes in the vanadium oxidation state from +4 to +2 in octahedral coordination. This allows the Mo^{6+} oxidation state to be preserved during Li insertion/deinsertion and, hereby, to avoid instabilities, which would result from lower oxidation states of Mo in tetrahedral coordination.

Experimental Section

1. Synthesis and Chemical Analysis. $Li_xV(MoO_4)_3$ ($x = 3$) powder was prepared from stoichiometric mixtures of Li_2MoO_4 (Alfa Aesar, 99%), MoO_3 (Alfa Aesar, 99.95%), and V_2O_3 (Alfa Aesar, 99.99%) in an argon atmosphere or in evacuated and sealed silica tubes at 813 K for 30 h. Single crystals of $Li_3V(MoO_4)_3$ for X-ray single crystal analysis were obtained from the synthesis of $Li_3V(MoO_4)_3$ at 1023 K in argon. The lithium content in $Li_xV(MoO_4)_3$ was varied between $x = 2$ and $x = 4$ by two different methods: (1) a chemical reaction at ambient temperature under an argon atmosphere[11,13] between $Li_3V(MoO_4)_3$ powder and either nitronium hexafluorophosphate (NO_2PF_6) in an acetonitrile medium as an oxidizing agent or *n*-butyllithium (LiC_4H_9) in *n*-heptane as a reducing agent or (2) in electrochemical cells. After syntheses, $Li_2V(MoO_4)_3$ and $Li_4V(MoO_4)_3$ were washed with acetonitrile or *n*-heptane, respectively, to remove traces of unreacted agents and dried under vacuum at room temperature. All attemps to synthesize $Li_2V(MoO_4)_3$ and $Li_4V(MoO_4)_3$ in quartz tubes gave a multiphase mixture of complex Li,Mo- and Li,V-oxides. The amounts of lithium, vanadium, and molybdenum in all prepared $Li_xV(MoO_4)_3$ compounds were determined quantitatively by the inductively coupled plasma−optical emission spectroscopy (ICP-OES) method (IRIS Intrepid II XUV, Thermo Fisher) using a 3:1 mixture of HCl (37%, p.a. Fa. Merck) and HNO_3 (65%, p.a. Fa. Merck) for dissolving the samples.

2. Crystal Structure Determination and Phase Analysis. The crystal structure of $Li_3V(MoO_4)_3$ was solved by single-crystal X-ray diffraction using the Xcalibur system from Oxford Diffraction. The software packages SHELXS[14] and SHELXL[15] were used for structure solution and refinement as included in X-STEP32.[16] A combined empirical absorption correction with frame scaling was applied, using the SCALE3 ABSPACK command in CrysalisRed.[17] Phase analysis and determination of cell parameters of $Li_xV(MoO_4)_3$ at room temperature were performed using powder X-ray diffraction (XRD) with a STOE STADI P diffractometer (Mo−Kα_1 radiation, $\lambda = 0.7093$ Å) in transmission mode. Phase analyses of $Li_xV(MoO_4)_3$ materials after electrochemical treatments were performed without any contact with air.

3. Thermal Analysis. The thermal behavior of synthesized $Li_2V(MoO_4)_3$, $Li_3V(MoO_4)_3$ and $Li_4V(MoO_4)_3$ compounds was investigated in a Model STA 449 apparatus (Netzsch, Selb, Germany), with respect to their phase reaction. Approximately 25 mg of powder was heated with the scan rate of 20 K/min in an alumina crucible from room temperature up to ~1070 K in a flowing argon atmosphere.

4. Electrochemical Characterization. Electrochemical studies on $Li_xV(MoO_4)_3$ cathode materials were performed with a multichannel potentiostatic−galvanostatic system VMP3 (Perkin−Elmer Instruments, Eden Prairie, MN) in standard Swagelok-type cells with metallic lithium as the anode material. For the positive electrode, a mixture of $Li_xV(MoO_4)_3$, carbon black, and poly(vinylidene fluoride) (PVDF) as a polymer binder in an 80:10:10 weight ratio was pressed onto 8-mm-diameter aluminum meshs and dried under vacuum at 100 °C. A 1 M solution of $LiPF_6$ in a mixture of ethylene carbonate (EC) and dimethylcarbonate (DMC) (1:1 v/v) was used as an electrolyte. The cells were assembled in an argon-filled glovebox with H_2O and O_2 contents of < 1 ppm.

5. In Situ Structural Investigations during Li Insertion and Extraction. In situ X-ray synchrotron diffraction measurements were performed at a synchrotron facility (HASYLAB/DESY, Hamburg, Germany, at beamline B2)[18] in transmission mode,

(9) Manthiram, A.; Goodenough, J. B. *J. Solid State Chem.* **1987**, *71*, 349–360.
(10) Begam, K. M.; Michael, M. S.; Prabaharan, S. R. S. *J. Solid State Electrochem.* **2008**, *12*, 971–977.
(11) Pop, N.; Pralong, V.; Caignaert, V.; Colin, J. F.; Malo, S.; Van Tendeloo, G.; Raveau, B. *Chem. Mater.* **2009**, *21*, 3242–3250.
(12) Smit, J. P.; McDonald, T. M.; Poeppelmeier, K. R. *Solid State Sci.* **2008**, *10*, 396–400.
(13) Wizansky, A. R.; Rauch, P. E.; DiSalvo, F. J. *J. Solid State Chem.* **1989**, *81*, 203–207.
(14) Sheldrick, G. M. *Acta Crystallogr., Sect. A: Found Crystallogr.* **1990**, *A46*, 467–473.
(15) Sheldrick, G. M. *SHELXL97 Program for the Refinement of Crystal Structures*; University of Göttingen: Göttingen, Germany, 1997.
(16) *X-STEP32*; Stoe & Cie GmbH: Darmstadt, Germany, 2000.
(17) *CrysalisRed, CCD Data Reduction GUI*, Version 1.171.26; Oxford Diffraction Poland Sp.: Wroclaw, Poland, 2005.
(18) Knapp, M.; Baehtz, C.; Ehrenberg, H.; Fuess, H. *J. Synchrotron Rad.* **2004**, *11*, 328–334.

using the OBI on-site readable image-plate detector[19] and a cell connected to a VMP multichannel galvanostat.[20] Data were collected in steps of 0.004° over the 2θ range of 4°−55°; a wavelength of 0.65110(1) Å was determined from the positions of eight reflections from LaB_6 reference material.

To characterize the starting material $Li_xV(MoO_4)_3$, a pattern was recorded before the electrochemical process was started. The cell was then successively charged and discharged in galvanostatic mode at a constant current, corresponding to the intercalation or deintercalation of one Li atom per formula unit over a period of 10 h (C/10). All diffraction patterns have been analyzed using the software package WinPLOTR.[21] The sequential design of the in situ cell requires phase-specific sample shifts during Rietveld refinements.[20] The aluminum foil, as the current collector on the cathode side, served as an internal standard during the measurements, and the refined lattice parameter of aluminum provided an independent control of the reliability of the obtained model parameters.

6. X-ray Photoelectron Spectroscopy (XPS). X-ray photoelectron spectroscopy (XPS) was applied to as-prepared $Li_3V(MoO_4)_3$ and to the products after electrochemical Li insertion or extraction. A PHI Model 5600 CI system with an Al Kα 350 W monochromatized X-ray source and a hemispherical analyzer at a pass energy of 29 eV were used. Two cells with pellets of the same cathode mixture consisting of $Li_3V(MoO_4)_3$, carbon black, and PVDF with a mass of ∼30 mg were charged and discharged with a C/10 rate to 4.9 V ($x \approx 2$) and 1.7 V ($x = 4$) and immediately disassembled. To remove $LiPF_6$ from the surface, the pellets were washed with DMC and scraped. During XPS measurements, when necessary, surface charging was minimized by means of a low-energy electron flood gun. The system base pressure was $\sim 10^{-9}$ mbar. The binding-energy scale was calibrated from minor carbon contaminations using the C 1s peak at 284.8 eV.

7. Magnetic Measurements. Magnetic properties of $Li_xV(MoO_4)_3$ ($x = 2$, 3, and 4) have been studied with a superconducting quantum interference device (SQUID) from Quantum Design. Measurements were performed in field-cooled and zero-field cooled mode in the temperature range of 1.8−350 K and with an external magnetic field strength of 500 G.

Results and Discussion

1. Synthesis and Sample Characterization. Brown-colored single-phase samples of $Li_3V(MoO_4)_3$ were obtained either in evacuated sealed silica tubes or in an argon flow at 813 K. At lower synthesis temperature (753−773 K), triclinic $Li_4Mo_5O_{17}$[22] was detected as a second phase, and its amount decreased with increasing temperature. A powder diffraction pattern of $Li_3V(MoO_4)_3$ is presented in Figure 1. All reflections can be explained based on the *Pnma* space group with lattice parameters $a = 5.0785(2)$ Å, $b = 10.4401(3)$ Å, $c = 17.5144(5)$ Å, $V = 928.63(5)$ Å^3, $Z = 4$ as a $Li_3Cr(MoO_4)_3$ isotype.[25]

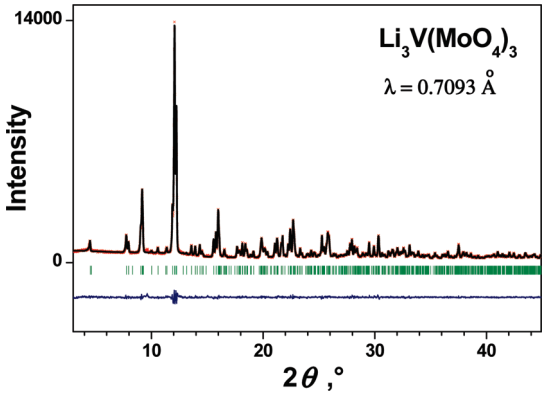

Figure 1. Measured and calculated powder diffraction pattern for $Li_3V(MoO_4)_3$, together with the difference curve (Mo $K\alpha_1$ radiation).

Single-phase samples of $Li_4V(MoO_4)_3$ with black color were prepared through the reaction of stoichiometric amounts (1:1) of $Li_3V(MoO_4)_3$ and LiC_4H_9 solution in *n*-heptane during 24 h, and its composition was confirmed by chemical analysis. No additional reflections were detected in the X-ray diffraction (XRD) pattern of $Li_4V(MoO_4)_3$, and the crystal structure is well-described, based on the same space group as $Li_3V(MoO_4)_3$ with the lattice parameters $a = 5.0915(2)$ Å, $b = 10.4497(3)$ Å, $c = 17.5401(5)$ Å, $V = 933.21(5)$ Å^3, and also $Z = 4$. The additionally inserted Li ions are clearly reflected by the expanded unit cell volume, but cannot be localized reliably during Rietveld refinement, because of the low scattering cross section of Li ions for X-rays. An excess of LiC_4H_9 and a longer reaction period led to a partial decomposition of $Li_3V(MoO_4)_3$ into Li_2MoO_4 and an unknown phase with cubic VO-type structure. Yellow-brown $Li_2V(MoO_4)_3$ was obtained without any impurity phase from the reaction between $Li_3V(MoO_4)_3$ and NO_2PF_6 in a molar ratio of 1:1. An excess of NO_2PF_6 led also to a phase decomposition: an analysis of the reaction products revealed the presence of $Li_xV(MoO_4)_3$ and $Li_4Mo_5O_{17}$. The lattice parameters of $Li_2V(MoO_4)_3$ are significantly smaller than those of $Li_3V(MoO_4)_3$: $a = 5.0584(3)$ Å, $b = 10.4330(4)$ Å, $c = 17.4328(7)$ Å, $V = 920.01(7)$ Å^3.

The differential thermal analysis (DTA) curves of $Li_xV(MoO_4)_3$ ($x = 2$, 3, and 4) show a decreasing of the thermal stability from $x = 3$ to $x = 4$ and $x = 2$ (see Figure 2). For $Li_3V(MoO_4)_3$, the melting temperature, accompanied by an endothermic signal at 903 K, and the crystallization temperature at 877 K were measured. The two endothermic signals during the heating of $Li_4V(MoO_4)_3$ may be interpreted as decomposition of the compound and the melting process, at ∼882 and 897 K, respectively. This was verified by XRD analysis of the $Li_4V(MoO_4)_3$ sample, which was heated in argon up to 990 K during 2 h and cooled to room temperature. Afterward, the presence of Li_2MoO_4, together

(19) Knapp, M.; Joco, V.; Baehtz, C.; Brecht, H. H.; Berghaeuser, A.; Ehrenberg, H.; von Seggern, H.; Fuess, H. *Nucl. Instrum. Methods, A* **2004**, *521*, 565–570.
(20) Nikolowski, K.; Baehtz, C.; Bramnik, N. N.; Ehrenberg, H. *J. Appl. Crystallogr.* **2005**, *38*, 851–853.
(21) Roisnel, T.; Rodriguez-Carvajal, J. *Mater. Sci. Forum* **2001**, *378*−381, 118–123.
(22) Wiesmann, M.; Weitzel, H.; Svoboda, I.; Fuess, H. *Z. Kristallogr.* **1997**, *212*, 795–800.
(23) Moulder, J. F.; Stickle, W. F.; Sobol, P. E.; Bomben, K. D. *Handbook of X-ray Photoelectron Spectroscopy*; Physical Electronics: Eden Prairie, MN, 1995.
(24) Jo, T. *J. Phys. Soc. Jpn.* **2003**, *72*, 155–159.
(25) Sarapulova, A.; Mikhailova, D.; Senyshyn, A.; Ehrenberg, H. *Solid State Chem.* **2009**, *182*, 3262–3268.

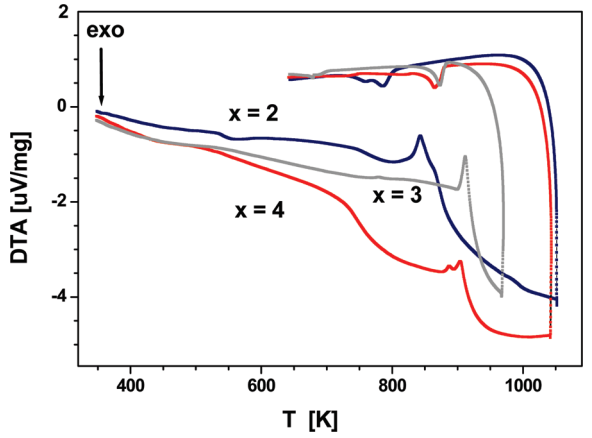

Figure 2. DTA data for $Li_xV(MoO_4)_3$ ($x = 2, 3, 4$): the phase with $x = 2$ was obtained through the reaction of $Li_3V(MoO_4)_3$ with NO_2PF_6, and the phase with $x = 4$ was obtained through the reaction of $Li_3V(MoO_4)_3$ with n-LiC_4H_9.

Table 1. Details of X-ray Single-Crystal Data Collection and Structure Refinement of $Li_3V(MoO_4)_3$

Crystal Data	
chemical formula	$Li_3VMo_3O_{12}$
formula weight	551.58
crystal system	orthorhombic
space group	*Pnma*
unit-cell dimensions	a = 5.0575(4) Å, b = 10.4562(10) Å, c = 17.5105(17) Å
cell volume	925.99(15) Å^3
Z	4
calculated density	3.956 g/cm^3
temperature	299(2) K
crystal form, color	prism, brown
crystal size	0.240 mm × 0.085 mm × 0.065 mm
Data Collection	
diffractometer	Oxford Diffraction Xcalibur; single-crystal X-ray diffractometer with sapphire CCD detector
data collection method	rotation method data acquisition using ω and φ scans (s)
radiation type	Mo Kα (λ = 0.71073 Å)
absorption coefficient	5.009 mm^{-1}
F(000)	1016
2θ range for data collection	2.27°−28.18°
ranges of h, k, l	$-6 \le h \le 5$, $-13 \le k \le 10$, $-18 \le l \le 23$
reflections collected/unique	3160/1096 [R(int) = 0.0272]
completeness to θ = 28.18°	91.0%
Refinement	
refinement method	full-matrix least-squares on F^2
number of data	1096
number of restraints	0
number of parameters	97
goodness-of-fit on F^2	1.133
final R indices [I > 2sigma(I)]	R_1 = 0.0248, wR_2 = 0.0757
R indices (all data)	R_1 = 0.0282, wR_2 = 0.0775
extinction coefficient	0.0058(5)
largest diff. peak and hole	1.096 and −1.200 e/Å^3

with an unknown phase, as major products and $Li_xV(MoO_4)_3$ as a minor phase was detected. A broad exothermic peak at ~884 K corresponds to the crystallization of $Li_4V(MoO_4)_3$. XRD analysis of $Li_3V(MoO_4)_3$ after the same heat treatment revealed practically pure $Li_3V(MoO_4)_3$. For $Li_2V(MoO_4)_3$, prepared through the reaction of $Li_3V(MoO_4)_3$ with NO_2PF_6, two endothermic signals during heating at 832 and 857 K also correspond to phase decomposition and melting. XRD analysis of $Li_2V(MoO_4)_3$ after DTA measurements showed the presence of complex V,Mo- and Li,V-containing oxides as major phases.

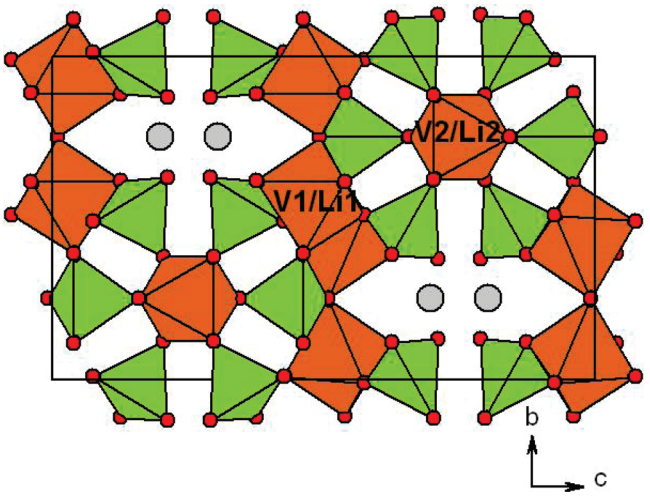

Figure 3. Crystal structure of $Li_3V(MoO_4)_3$, view on the *bc*-plane. Coordination polyhedra for V and some Li atoms are octahedra; other Li atoms (as gray spheres) are situated in channels with larger Li−**O distances.**

Table 2. Positional Parameters and Equivalent Isotropic Displacement Parameters for $Li_3V(MoO_4)_3$

atom	site	x	y	z	U_{iso} (Å^2)	occupancy
Mo(1)	4*c*	0.2213(1)	−0.25	0.0574(1)	0.0011(1)	1
Mo(2)	8*d*	0.2784(1)	−0.0262(1)	−0.1562(1)	0.0011(1)	1
V(1)	4*c*	0.6097(4)	0.25	−0.2495(1)	0.0016(1)	0.44(1)
Li(1)	4*c*	0.6097(4)	0.25	−0.2495(1)	0.0016(1)	0.56(1)
V(2)	8*d*	0.7532(3)	−0.0710(2)	−0.0256(1)	0.0013(1)	0.30(1)
Li(2)	8*d*	0.7532(3)	−0.0710(2)	−0.0256(1)	0.0013(1)	0.70(1)
Li(3)	4*c*	0.7490(20)	−0.25	−0.1960	0.0025(2)	1
O(1)	8*d*	0.3580(6)	0.1187(3)	−0.2052(2)	0.0016(1)	1
O(2)	8*d*	0.0809(6)	−0.1225(3)	−0.2129(2)	0.0021(1)	1
O(3)	8*d*	0.5607(6)	−0.1128(3)	−0.1260(2)	0.0017(1)	1
O(4)	8*d*	0.4219(5)	−0.1159(3)	0.0374(2)	0.0018(1)	1
O(5)	4*c*	0.1388(9)	−0.25	0.1555(2)	0.0018(1)	1
O(6)	8*d*	0.0798(6)	0.0103(3)	−0.0747(2)	0.0017(1)	1
O(7)	4*c*	−0.0562(8)	−0.25	−0.0056(2)	0.0017(1)	1

2. Crystal Structure Determination. According to the single-crystal X-ray diffraction data (see Table 1), $Li_3V(MoO_4)_3$ is isostructural to $NaCo_{2.31}(MoO_4)_3$.[7] From a structural point of view, the composition $Li_3V(MoO_4)_3$ can be better described as $AB_2C(MoO_4)_3$ with A = $V_{0.44}Li_{0.56}$, B = $V_{0.30}Li_{0.70}$, and C = Li.

In the structure, there are two types of (Li,V)-octahedra: infinite chains of face-sharing AO_6 along the [100] axis (metals on the 4*c* site) and networks of corner- and edge-sharing BO_6 parallel to the (001) plane with a metal on the 8*d* site (see Figure 3; details regarding the position parameters of $Li_3V(MoO_4)_3$ are given in Table 2). The isolated MoO_4 tetrahedra connect networks and chains via corners into a pseudo-hexagonal framework with channels parallel to [100], which are occupied only by Li atoms. The average Li−O distances are 2.044(4) Å and 2.084(4) Å for mixed $(Li,V)O_6$ octahedra and 2.175(9) Å for Li atoms in the channels (Figure 3) for LiO_6 trigonal prisms. Li atoms in channels occupy only 4*c* positions, forming so-called "ordering" in the structure with half-filled channels.

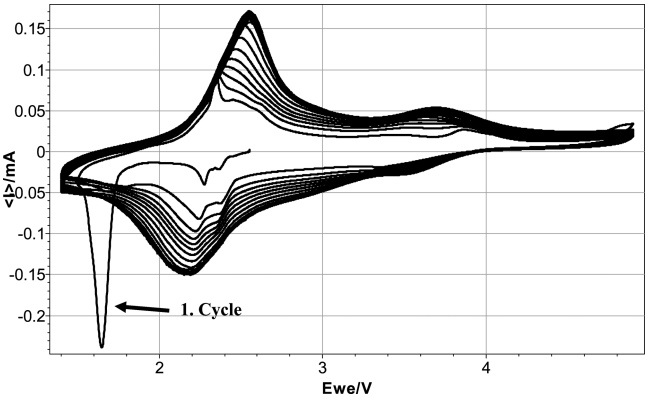

Figure 4. Cyclic voltammetry curves at a voltage sweep rate of 0.1 mV/s for $Li_3V(MoO_4)_3$.

3. Electrochemical Behavior of $Li_3V(MoO_4)_3$. *3.1. Cyclic Voltammetry (CV) Measurements.* Some reduction and oxidation processes were registered during cyclic voltammetry measurements of the electrochemical cell with $Li_3V(MoO_4)_3$ cathode, cycled with a voltage sweep rate of 0.1 mV/s between 1.4 V and 4.9 V (see Figure 4). Different electrochemical behavior was observed during the first and following discharge cycles: a strong reduction peak was detected at ~1.7 V in the first cycle, which has completely disappeared in the third one (Figure 4). For all cycles, three reproducible oxidation−reduction processes, corresponding to the insertion and extraction of Li atoms, were observed. From two reduction peaks at 2.3−2.4 V and from two oxidation peaks at 2.3−2.5 V, one can conclude a two-step process of Li insertion/deinsertion in $Li_3V(MoO_4)_3$ with $Li_{3+x}V(MoO_4)_3$ formation. Li deinsertion from $Li_3V(MoO_4)_3$ forming $Li_{3-x}V(MoO_4)_3$ is also reversible and occurs at 3.7 V.

3.2. Galvanostatic Cycling with Potential Limitation (GCPL). Galvanostatic experiments with a C/10 rate showed that about two Li atoms can be reversibly inserted and deinserted in $Li_xV(MoO_4)_3$ between 1.5 and 4.5 V (see Figure 5a). The first charge is quite different from the next ones, having three pronounced plateaus at 2.2, 2.3, and 1.7 V, which are smoothed or disappear in the successive ones. XRD patterns from the cathode materials after the first cycle and after 30 cycles, respectively, are very similar and reveal, besides $Li_xV(MoO_4)_3$ (90% w/w), the presence of cubic "$Li_{3.2}Mo_{0.8}O_4$" (6%) (a = 4.1675(5) Å, $Fm\bar{3}m$) and trigonal Li_2MoO_4 (4% w/w) (a = 14.339(2) Å, c = 9.568(2) Å, $R\bar{3}$). Therefore, the formation of "$Li_{3.2}Mo_{0.8}O_4$" and Li_2MoO_4 seems to occur already primarily in the first cycle. Ex situ structure investigation of the $Li_3V(MoO_4)_3$ cathode material after cell discharge down to 1.6 V and an immediate disassembling of the cell under an argon atmosphere in a glovebox confirmed the formation of "$Li_{3.2}Mo_{0.8}O_4$" during the first discharge cycle (see Figure 6). The reflections of $Li_{3.2}Mo_{0.8}O_4$ disappeared when the cell was discharged down to 1.5 V in the first cycle and left in open circuit voltage (OCV) mode for 12 h. The cell voltage increased up to 2.2 V, which corresponds to the initial voltage of $Li_4V(MoO_4)_3$ cathode material, obtained through the reaction with n-LiC_4H_9. The actual composition of the "$Li_{3.2}Mo_{0.8}O_4$"-like phase with a cubic rocksalt-type structure

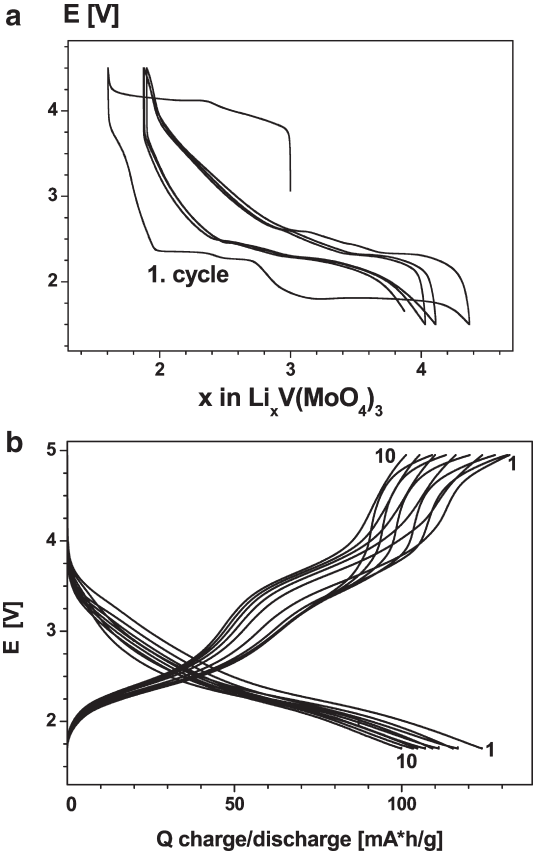

Figure 5. Galvanostatic cycling of $Li_3V(MoO_4)_3$/Li cells between (a) 4.4 and 1.6 V (C/10) and (b) 4.9 and 1.8 V (C/10). In panel (a), the first charge cycle is different from the following ones and reflects a conditioning process of the material.

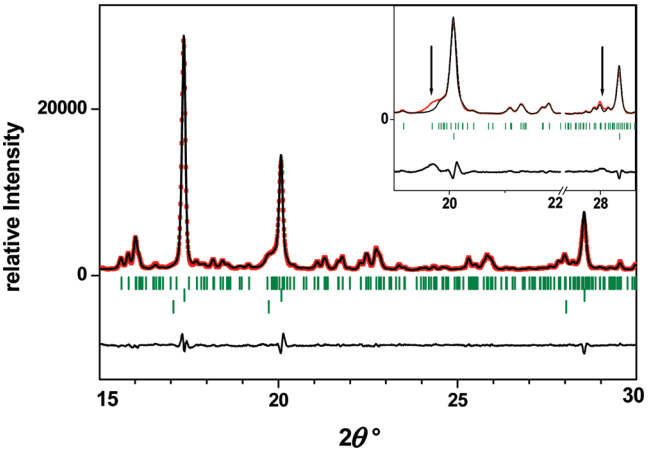

Figure 6. Section of the XRD pattern of $Li_xV(MoO_4)_3$ material, discharged down to 1.6 V; observed and calculated profiles, together with their difference curve, are shown. Tick marks represent from top to bottom the positions of reflections for orthorhombic $Li_xV(MoO_4)_3$, Al from the aluminum mesh, and cubic "$Li_{3.2}Mo_{0.8}O_4$". The inset shows results of a Rietveld refinement for a two-phase model, including only $Li_xV(MoO_4)_3$ and Al contributions, demonstrating the presence of a third crystalline phase.

is not clear. According to the structural model,[27] Li and Mo are randomly distributed on the same crystallographic site and have an octahedral coordination of O atoms. In the "$Li_{3.2}Mo_{0.8}O_4$"-like phase, formed after the galvanostatic cycling, V atoms could also be partially

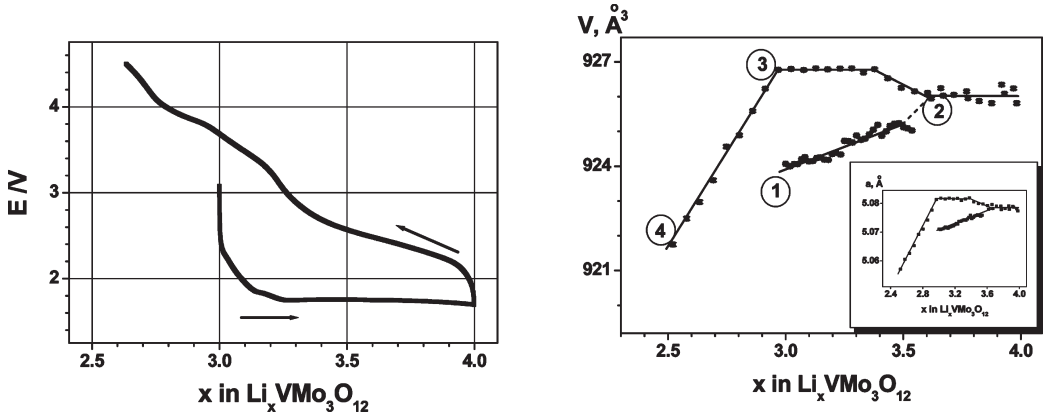

Figure 7. In situ synchrotron diffraction experiment on $Li_3V(MoO_4)_3$ as cathode material in an electrochemical test cell during CCPL at C/10. Left: the cell was at first discharged down to 1.7 V and then was charged up to 4.5 V. Right: dependence of the lattice volume of $Li_xV(MoO_4)_3$ on lithium content during galvanostatic cycling. Detailed structural data for points 1−**4 are presented in Table 3.**

included in the structure, which can reflect the slightly larger lattice parameter, in comparison with $Li_{3.2}Mo_{0.8}O_4$ (a = 4.14 Å).[27]

The appearance of a second phase with a rocksalt-type structure and a cell parameter a = 4.15 Å was also detected after the reaction between $Fe_2(MoO_4)_3$ and an excess of n-LiC_4H_9, leading to $x > 2$ in $Li_xFe(MoO_4)_3$:[9] the authors proposed an existence of a solid solution between $Fe_{1-\delta}O$ and Li_2MoO_3. More-complicated behavior during cell discharge was registered for $Li_3Fe(MoO_4)_3$:[3] XRD data of $Li_3Fe(MoO_4)_3$ cathode material discharged down to 1 V revealed a complete decomposition of the NASICON-type structure of $Li_3Fe(MoO_4)_3$ into cubic $Li_{2y}Mo(IV)Fe(II)_2O_{2+3y}$ (a = 4.15 Å) with a rocksalt-type structure and amorphous lithium molybdate $Li_{8-2y}Mo(IV)_{3-y}O_{10-3y}$, which transforms to Li_2MoO_4 after exposure to air.

$Li_{8-2y}Mo(IV)_{3-y}O_{10-3y}$ should be responsible for reversible Li insertion/deinsertion during the cell cycling between 4 V and 1 V, that corresponds to the insertion of three Li^+ ions [2] at an average voltage of ~2 V.

It was also shown[2] that a test cell with isostructural $Li_{3+x}Fe(MoO_4)_3$ cathode material can be reversibly cycled in the voltage window of 3−1.6 V with a large plateau at 2.4 V, corresponding to the iron reduction $Fe^{3+} \rightleftharpoons Fe^{2+}$. Upon lithium insertion in the compositional range $0 \le x \le 1$ two two-phase regions were detected between $x = 0$ and $x = 0.75$, and $x = 0.75$ and $x = 1.0$. The crystal structures of single-phase $Li_xFe(MoO_4)_3$ (x = 0.75, 1) are derived from the one of $Li_3Fe(MoO_4)_3$ by completely filling the channels along the a-axis successively.

In the case of $Li_3V(MoO_4)_3$ the plateau at 1.7 V could correspond to the reduction of vanadium $V^{3+} \rightleftharpoons V^{2+}$ as observed for example for the discharge of NASICON-type $Li_3V_2(PO_4)_3$ at 1.7 V,[1] or to the reduction of molybdenum $Mo^{6+} \rightleftharpoons Mo^{5+}$. Although a small amount of a rocksalt-type phase appears during cell discharge, it does not seem to contribute significantly to electrochemical reduction, because this phase disappears or becomes amorphous during charging, while the NASICON-type $Li_xV(MoO_4)_3$ is still observed after 30 cycles over the voltage range from 4.8 V to 1.6 V.

The reflections from the $Li_3V(MoO_4)_3$ cathode material after cycling are much broader in comparison with the pristine material, which indicates a smaller average crystallite size of 160 nm instead of several μm in pristine $Li_3V(MoO_4)_3$. The capacity loss during cycling (Figure 5b) could be attributed to poorer electronic and ionic conductivity, because of a contact loss caused by the ongoing breaking of crystallites.

4. In Situ Synchrotron Diffraction. Two compositions, $Li_3V(MoO_4)_3$ and $Li_4V(MoO_4)_3$, were taken for detailed structural investigations upon Li insertion and deinsertion. The electrochemical cell with $Li_3V(MoO_4)_3$ was first discharged down to 1.7 V with a C/10 rate, which corresponds to the insertion of one Li per formula unit and then charged up to 4.5 V, corresponding to a total lithium content of ~2.6 (see Figure 7). The electrochemical cell with $Li_4V(MoO_4)_3$ was charged up to 4.9 V with a C/10 rate, which led to a decrease in the lithium content down to x = 2.3 (see Figure 8). All observed reflections during Li insertion/extraction in the first cycle are well-explained by the presence of $Li_xV(MoO_4)_3$, Li_2MoO_4, and "$Li_{3.2}Mo_{0.8}O_4$". The evolutions of cell volume and unit-cell parameters a and c with lithium content are very similar (Figure 7) and can be explained by the scheme of Li insertion/deinsertion into the channels along the a-axis within the $Li_xV(MoO_4)_3$ structure (see Figure 9).

A monotonous increase of the unit cell volume and the a and c lattice parameters was observed up to a lithium content of x = 3.5 per formula unit, confirming a topotactic single-phase mechanism for Li insertion. (See Figure 10.) Additional reflections from "$Li_{3.2}Mo_{0.8}O_4$" appeared for higher lithium contents, while the lattice parameters of $Li_xV(MoO_4)_3$ did not change anymore significantly (see Figure 7). A multiphase mechanism is indicated, supported by the long plateau at 1.7 V (Figure 7, left): either the formation of structurally related phases $Li_xV(MoO_4)_3$ with very similar lattice parameters

(26) Panin, R. V.; Schpanchenko, R. V.; Mironov, A. V.; Velikodny, Y. A.; Antipov, E. V.; Hadermann, J.; Tarnopolsky, V. A.; Yaroslavtsev, A. B.; Kaul, E. E.; Geibel, C. *Chem. Mater.* **2004**, *16*, 1048–1055.
(27) Blasse, G. *Z. Anorg. Allg. Chem.* **1964**, *331*, 44–50.

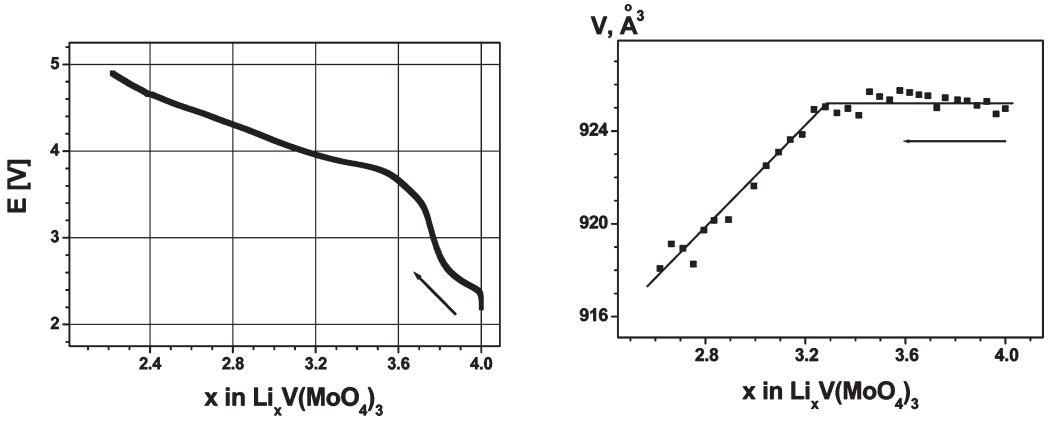

Figure 8. In situ synchrotron diffraction experiment on $Li_4V(MoO_4)_3$, obtained from the chemical reaction of $Li_3V(MoO_4)_3$ with LiC_4H_9, in an electrochemical test cell during cell charge up to 4.9 V at C/10 (left). Right: dependence of lattice volume of $Li_xV(MoO_4)_3$ on lithium content during cell charge.

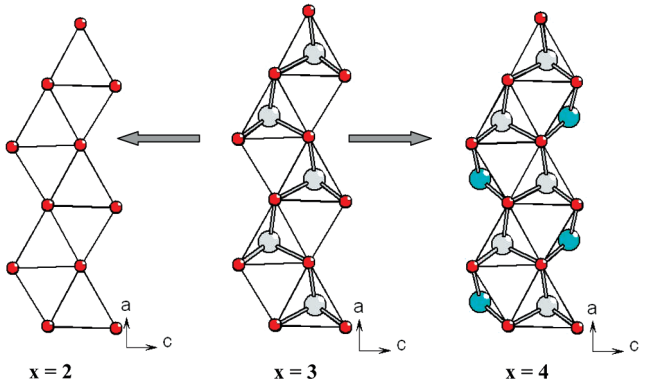

Figure 9. Scheme of Li insertion/deinsertion into channels along the *a*-axis in the $Li_xV(MoO_4)_3$ structure.

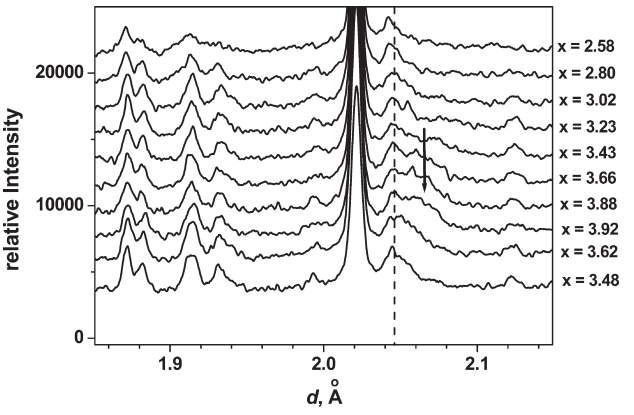

Figure 10. Section of the in situ synchrotron powder diffraction patterns (λ = 0.65110(1) Å) of $Li_xV(MoO_4)_3$ during Li intercalation (from x = 3.48 to x = 3.92) and deintercalation (down to x = 2.58). Between x = 3.62 and x = 3.02, a reflection at d = 2.045 Å indicates the formation of a new phase, which disappears again at lower x values. Higher-quality ex situ data revealed that this intermediate phase is in good agreement with a cubic "$Li_{3.2}Mo_{0.8}O_4$"-type phase.

but a different distribution of lithium, as in the case of $Li_3Fe(MoO_4)_3$,[3] or the partial decomposition of $Li_xV(MoO_4)_3$ into a cubic Li,(V),Mo-oxide and Li_2MoO_4. It is rather improbable that Li_2MoO_4 intercalates Li atoms in the channels, because, according to the work in ref 28, a lithiation of Li_2MoO_4 was first observed at <1 V and it is not accompanied by the formation of a distinct plateau. The reflections of "$Li_{3.2}Mo_{0.8}O_4$" disappeared again during the following Li deinsertion below $x \approx 3$. A plateau in the unit-cell volume versus lithium content was observed during the charge of a test cell with a cathode either from $Li_3V(MoO_4)_3$ after discharge to $x = 4$ or from $Li_4V(MoO_4)_3$ material obtained from the reaction with LiC_4H_9, which indicates a two-phase mechanism of lithium extraction in the region from $x \approx 4$ down to $x \approx 3$. These mechanisms are supported by the observed hysteresis between states 1 and 2 on one hand and states 2 and 3 on the other (see Figure 7, right). The first process is a topotactic Li insertion with a one-phase mechanism, but the Li extraction occurs via a two-phase mechanism.

Li insertion/deinsertion in $Li_xV(MoO_4)_3$ must affect interatomic distances and polyhedral distortions in Li,VO_6 octahedra and MoO_4 tetrahedra. The average interatomic distances and polyhedral distortions, defined as $\eta = [d(M-O)_{max} - d(M-O)_{min}]/\overline{d(M-O)}$, are presented in Table 3 for four composition states, labeled 1−4 in Figure 7.

For the pristine composition $Li_3V(MoO_4)_3$ (state 1), the smallest degrees of distortions are found and reflect the highest structural stability among all $Li_xV(MoO_4)_3$ compositions. Face-sharing $Li,V(1)O_6$ octahedra are more rigid than $Li,V(2)O_6$ octahedra (see Figure 3), connected via corners and edges only. During oxidation or reduction, the polyhedral distortions increase for all polyhedra. The oxidation is mainly due to the transition $V^{3+} \rightleftharpoons V^{4+}$, whereas two different processes can be discussed during reduction: $V^{3+} \rightleftharpoons V^{2+}$ or $Mo^{6+} \rightleftharpoons Mo^{5+}$. During Li insertion from $x \approx 3$ to $x \approx 4$, the average interatomic distances increase for MoO_4 tetrahedra to 1.87(1) Å from 1.837(7) Å for $Mo(1)O_4$ and 1.852(9) Å for $Mo(2)O_4$, which could mean a partial reduction of Mo(VI) to Mo(V). However, simultaneously, the average V,Li−O interatomic bond length becomes shorter. During the following Li extraction down to $x \approx 3$, the polyhedra distortion decrease but do not reach their initial lowest values. The decrease of one V(2)−O bond down to 1.80(2) Å in $Li_{2.65}V(MoO_4)_3$ might reflect a tendency of V ions to form a short vanadyl bond

(28) Leyzerovich, N. N.; Bramnik, K. G.; Buhrmester, T.; Ehrenberg, H.; Fuess, H. *J. Power Sources* **2004**, *127*, 76–84.

Table 3. Structural Details Obtained from In Situ Synchrotron Diffraction for $Li_xV(MoO_4)_3$ during the First Discharge/Charge Cycle

$d_{(Li,V(1)-O)}$ (Å and η)	$d_{(Li,V(2)-O)}$ (Å and η)	$d_{(Mo(1)-O)}$ (Å and η)	$d_{(Mo(2)-O)}$ (Å and η)
	$Li_3V(MoO_4)_3$, 3.2 V		
2.06(1)	2.091(8)	1.804(7)	1.834(10)
2.006(8) × 2	1.927(9)	1.824(7)	1.817(7)
2.00(1)	2.116(6)	1.850(7)	1.847(7)
1.961(8) × 2	2.045(8)	1.870(7)	1.879(10)
	1.919(9)		
	2.156(8)		
η = 0.02	**η = 0.12**	**η = 0.04**	**η = 0.02**
	$Li_4V(MoO_4)_3$, 1.7 V		
1.81(2)	1.86(2)	1.74(1)	1.84(2)
2.07(2) × 2	1.86(2)	1.85(1)	1.85(1)
2.07(2)	1.86(2)	1.86(1)	1.85(1)
1.94(2) × 2	2.04(2)	2.03(1)	1.95(2)
	2.20(2)		
	2.39(2)		
η = 0.13	**η = 0.26**	**η = 0.16**	**η = 0.06**
	$Li_3V(MoO_4)_3$, 3.7 V		
2.01(2)	1.88(2)	1.83(1)	1.80(1)
1.97(1) × 2	1.90(2)	1.84(1)	1.80(1)
2.13(2)	2.02(2)	1.90(1)	1.895(9)
1.94(1) × 2	2.10(2)	1.90(1)	1.90(1)
	2.14(1)		
	2.20(2)		
η = 0.10	**η = 0.16**	**η = 0.04**	**η = 0.05**
	$Li_{2.65}V(MoO_4)_3$, 4.5 V		
1.94(3)	1.80(2)	1.82(1)	1.66(2)
1.87(2) × 2	1.87(2)	1.95(1)	1.80(2)
2.16(2)	2.03(2)	1.95(1)	1.90(1)
1.99(2) × 2	2.16(2)	2.00(1)	1.90(1)
	2.28(2)		
	2.28(2)		
η = 0.15	**η = 0.23**	**η = 0.09**	**η = 0.13**

typical for V^{4+}. For example, a bond length of ~1.64 Å was observed for the α-and β-polymorphs of $Na_4VO(PO_4)_2$.[26] The random distribution of Li ions on the 4*c* site in $Li_xV(MoO_4)_3$ probably disturbs a further decrease of the average (V,Li)−O bond and might be responsible for the lower capacity, in comparison with the theoretical value, corresponding to Li extraction down to $x \approx 2$.

5. XPS Studies. The changes of the electronic structure due to Li insertion and extraction were studied by "quasi in situ" XPS[29] (see Figure 11a−c). Although the XPS method represents the electronic structure of the surface region only and is influenced by contaminations or surface effects, a presence of V^{3+} and Mo^{6+} in $Li_xV(MoO_4)_3$ with $x = 3$, according to the V 2p and Mo 3d emission peak positions, can be concluded, in agreement with reference data in the literature.[23] A shift of the V 2p peak (Figure 11a) toward higher energies for $x = 2$, as well as the appearance of an additional peak at a lower energy in the Mo3d subspectrum (Figure 11b) for $x = 4$, unambiguously correspond to an increase in the average V oxidation state after Li extraction and a decrease in the average Mo oxidation state after Li insertion. A slight shift of the V 2p peak toward smaller energies for $x = 4$ could indicate that a small amount of V ions can be assigned to a formal oxidation state lower than +3. The Mo 3d peaks for $x = 4$ are somewhat broader, in comparison to those for $x = 3$ (Figure 11b), indicating a change of Mo−O bond strength during Li insertion. Although O 1s peaks could represent a superposition of oxygen contributions from $Li_xV(MoO_4)_3$ and traces of DMC, which was used for sample washing after electrochemical experiments, they became significantly broader and are shifted to higher energies from $Li_2V(MoO_4)_3$ to $Li_4V(MoO_4)_3$ (Figure 11c). It corresponds to a strengthening of a covalence Li−O bonding due to partial charge transfer from O ions to Li ions in the channels with an increasing degree of Li occupation on this site. The Mo 3d spectrum of $Li_3V(MoO_4)_3$ after 20 charge/discharge cycles between 1.4 V and 4.9 V (Figure 4),

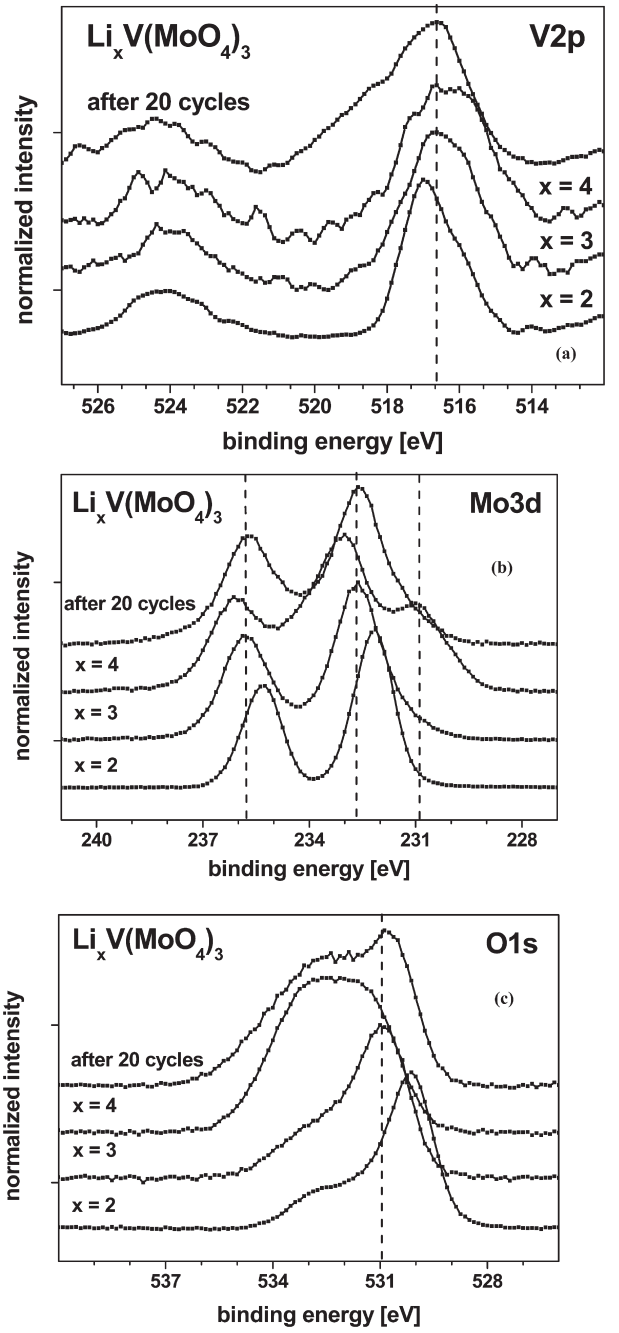

Figure 11. (a) V 2p, (b) Mo 3d, and (c) O 1s core peaks of $Li_xV(MoO_4)_3$ ($x = 2, 3, 4$ and after 20 cycles between 1.4 V and 4.9 V). $Li_2V(MoO_4)_3$ and $Li_4V(MoO_4)_3$ were prepared in electrochemical test cells.

(29) Oswald, S.; Nikolowski, K.; Ehrenberg, H. *Anal. Bioanal. Chem.* **2009**, *393*, 1871–1877.

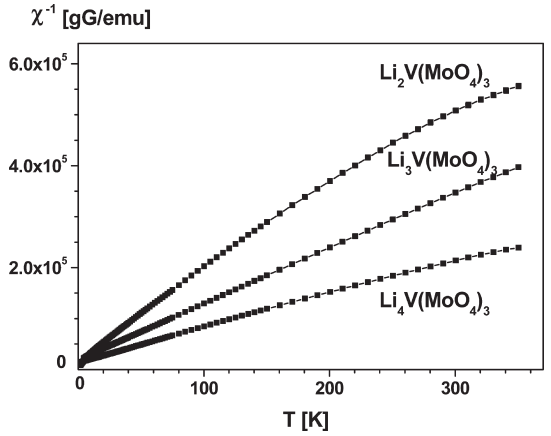

Figure 12. Temperature dependence of the inverse magnetic susceptibility for $Li_xV(MoO_4)_3$ ($x = 2, 3, 4$).

Table 4. Magnetic Properties of $Li_xV(MoO_4)_3$ ($x = 2, 3, 4$)[a]

compound	χ_0 ($\times 10^7$ emu/gG)	θ (K)	μ_{eff}(exp) (μ_B)	temperature range for fit (K)
$Li_2V(MoO_4)_2$	4.8(8)	−5.4(3)	1.143(9)	10−350
$Li_3V(MoO_4)_3$	−0.08(1)	−17.9(1)	2.026(1)	15−350
$Li_4V(MoO_4)_3$	−1.6(2)	−19.8(4)	2.55(2)	6−320

[a] $Li_4V(MoO_4)_3$ was prepared from $Li_3V(MoO_4)_3$ through the reaction with n-LiC_4H_9, $Li_2V(MoO_4)_3$ was obtained in the electrochemical test cell. The compositions were confirmed by ICP-OES. The standard deviations in brackets are determined as the limits, for which an up to 10% higher residual is obtained in the least-squares fit than for the optimum fit for eq 1.

followed by a voltage relaxation for 12 h, to reach an equilibrium state, resembles the spectrum of pristine material $Li_3V(MoO_4)_3$ and does not demonstrate a shoulder at ~231 eV, excluding any presence of Mo in a lower oxidation state than +6. This confirms the reversibility of the proposed Mo reduction during Li insertion.

6. Magnetic Measurements. According to the magnetic measurements, $Li_xV(MoO_4)_3$ ($x = 2, 3, 4$) compositions are paramagnetic, down to 1.9 K (see Figure 12). $Li_4V(MoO_4)_3$ was prepared from $Li_3V(MoO_4)_3$ through the reaction with n-LiC_4H_9, $Li_2V(MoO_4)_3$ was obtained in the electrochemical test cell. The compositions were confirmed by ICP-OES. Paramagnetic moments and paramagnetic Curie−Weiss temperatures (θ), calculated from fitting eq 1 to the observed data, are presented in Table 4.

$$\chi(T) = \frac{C}{T-\theta} + \chi_0 \qquad (1)$$

Slightly negative values for θ indicate weak antiferromagnetic interactions. With increasing lithium content, they become stronger and the paramagnetic moments larger. By assuming that V^{4+} ($3d^1$) and V^{3+} ($3d^2$) exist in $Li_2V(MoO_4)_3$ and $Li_3V(MoO_4)_3$, respectively, the experimental paramagnetic moments (Table 4) are smaller than the calculated "spin-only" values for a $3d^1$ electronic configuration (1.73 μ_B) and a high-spin $3d^2$ electronic configuration (2.83 μ_B). This could be a result of strong antiparallel spin−orbit couplings or an intermediate spin state for V^{3+} in $Li_3V(MoO_4)_3$. It is known[24] that, in vanadium perovskites with $V^{+3}O_6$ octahedra, the orbital magnetic moment is strongly coupled to the spin and reduces the total moment by ~1 μ_B. For $Li_4V(MoO_4)_3$, V and Mo ions should contribute to the total paramagnetic moment. According to a very simple ionic model, based on V^{3+} and Mo contributions only, and using the experimental value from $Li_3V(MoO_4)_3$ as an approximation for the V^{3+} paramagnetic moment, the effective paramagnetic moment of Mo is estimated by eq 2 and gives 1.50 μ_B.

$$\mu(\mathrm{Mo}) = \sqrt{\mu^2_{exp} - \mu^2(V^{3+})} \qquad (2)$$

This value is smaller than the spin-only value for Mo^{5+} (1.73 μ_B) and in agreement with a partially reduced oxidation state, in comparison with Mo^{6+}. In contrast, the existence of V^{2+}/Mo^{6+} pairs in $Li_4V(MoO_4)_3$ with only V^{2+} ($3d^3$) and diamagnetic Mo^{6+} would give a "spin-only" paramagnetic moment of ~3.8 μ_B, which is too high.

Conclusion

$Li_3V(MoO_4)_3$ is a suitable material for both Li insertion and extraction with preserving the underlying NASICON-type crystal structure. Li ions can be topotactically intercalated in $Li_3V(MoO_4)_3$ forming "$Li_xV(MoO_4)_3$" with $x \approx 4$ by a chemical route or in an electrochemical test cell. In the first discharge cycle, Li insertion at 1.7 V is accompanied by a partial decomposition of $Li_3V(MoO_4)_3$ to trigonal Li_2MoO_4 and an unknown phase with a cubic rocksalt-type structure. It is rather improbable that Li_2MoO_4 participates in the electrochemical processes at this relatively high voltage. A multiphase insertion mechanism of Li in $Li_xV(MoO_4)_3$ from $x = 3.5$ to $x = 4$ could remain topotactical and be similar to that in $Li_3Fe(MoO_4)_3$,[3] including the formation of structurally related phases $Li_xV(MoO_4)_3$ with very similar lattice parameters but a different distribution of Li on initially vacant sites. Ex situ neutron diffraction data from partially lithiated $Li_{3+x}V(MoO_4)_3$ materials are nessesary in combination with high resolution in situ synchrotron diffraction studies on $Li_3V(MoO_4)_3$ after one complete cycle to reveal the details of this mechanism. In contrast to $Li_3Fe(MoO_4)_3$, the Li insertion in $Li_{3+x}V(MoO_4)_3$ is accompanied mostly by a reduction of Mo^{6+} and partially of V^{3+} ions, in agreement with the resulting paramagnetic moments.

Acknowledgment. This work was financially supported by the Deutsche Forschungsgemeinschaft (DFG) and benefited from access to the beamline B2 at the Hamburger Synchrotronstrahlungslabor at DESY, Germany. The authors are indebted to Prof. R. Glaum (Institut für Anorganische Chemie, Universität Bonn, Germany) for fruitful discussion.

Supporting Information Available: CIF data for $Li_xV(MoO_4)_3$. This material is available free of charge via the Internet at http://pubs.acs.org.